Shuttle-promoted nano-mechanical current switch

Taegeun Song,[1,a)] Leonid Y. Gorelik,[2] Robert I. Shekhter,[3] Mikhail N. Kiselev,[1] and Konstantin Kikoin[4]
[1]*Condensed Matter and Statistical Physics Section, The Abdus Salam International Center for Theoretical Physics, I-34151 Trieste, Italy*
[2]*Department of Applied Physics, Chalmers University of Technology, SE-412 96 Göteborg, Sweden*
[3]*Department of Physics, University of Gothenburg, SE-412 96 Göteborg, Sweden*
[4]*School of Physics and Astronomy, Tel-Aviv University, Tel-Aviv 69978, Israel*

(Received 1 June 2015; accepted 9 September 2015; published online 21 September 2015)

We investigate electron shuttling in three-terminal nanoelectromechanical device built on a movable metallic rod oscillating between two drains. The device shows a double-well shaped electromechanical potential tunable by a source-drain bias voltage. Four stationary regimes controllable by the bias are found for this device: (i) single stable fixed point, (ii) two stable fixed points, (iii) two limit cycles, and (iv) single limit cycle. In the presence of perpendicular magnetic field, the Lorentz force makes possible switching from one electromechanical state to another. The mechanism of tunable transitions between various stable regimes based on the interplay between voltage controlled electromechanical instability and magnetically controlled switching is suggested. The switching phenomenon is implemented for achieving both a reliable *active* current switch and sensoring of small variations of magnetic field. © *2015 AIP Publishing LLC*.
[http://dx.doi.org/10.1063/1.4931458]

Nanoelectromechanical (NEM) systems arouse interest not only due to diverse potential applications as nano-devices but also as an efficient constituent of modern nano-electronics.[1,2] While the NEM coupling plays an important part in electronic transport through nano-devices, the charge transport associated with the nano-mechanical motion demonstrates various interesting quantum effects such as Coulomb blockade,[3] resonant tunneling,[4] current blockade,[5] spin-dependent transport,[6] Franck-Condon blockade,[7] and so on. Besides, strong NEM coupling provides very efficient ways to control electronic and mechanical degrees of freedom of NEM-devices. The confined area of movable nanometer sized island of electron gas (quantum dot) is characterized by quantized energy spectrum. The quantum mechanical tunneling between the source/drain and quantum dot is responsible for a one-by-one electron charge transfer. Such electron transport by periodically moving quantum dot is known as "shuttling phenomenon."[8,9] The signature of shuttling was experimentally demonstrated in Refs. 10–13.

Recent experimental work[14] suggested a new type of a three-terminal NEM-device as a current switch controlled by shifting the frequency of input signal. The "Y-switch" device consisted of three electric terminals and mechanical shuttle component—metallic island on top of nano-pillar mechanical resonator.[14] The three-terminal device demonstrated tunable mechanical modes operating in radio-frequency (RF) regime at room temperatures. The applications of this type of NEM-based device for quantum information processing potentially include (but not limited to) frequency dependent RF switches and ultra low-power logic elements. In our theoretical work, we propose an idea of another three-terminal device where mechanical resonator plays also a part of one of electric terminals. We suggest a mechanism of controlling the switching regime by magnetic field. The high sensitivity of NEM resonator provides an opportunity to manipulate the charge transfer in the situation when the state of device is defined by out of equilibrium conditions. These systems are referred as "active NEM devices."

In this work, we consider a NEM system containing a cantilever of length L as a source located at the symmetric point between two vertical drains separated by the air gap of width $2D$ as shown in Fig. 1(a). Equivalent circuit model for tunnel junction (Fig. 1(b)) is combined with Newtonian dynamics of the cantilever. First, we describe mechanical degrees of freedom of the cantilever by the displacement $u(z)$ characterizing the cantilever deflection from the straight configuration at the point z (that is, the cantilever axis with its origin at the fixed end, see Fig. 1(a)). Second, we introduce the eigenmode representation for the cantilever displacement[15] and characterize the *fundamental mode* of the

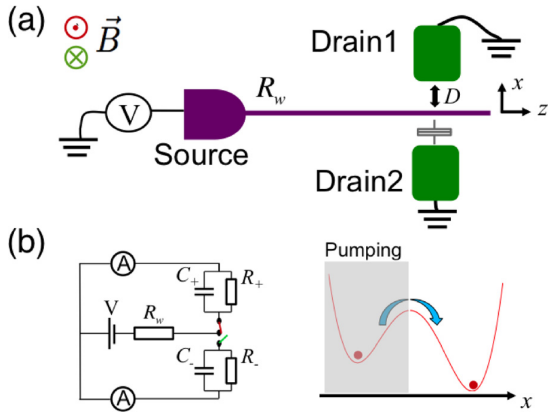

FIG. 1. (a) Schematic figure of the system we consider. (b) Equivalent electric circuit (left panel) and electromechanical potential $U_{\text{eff}}(x)$ in the presence of perpendicular magnetic field (right panel).

a)Electronic mail: tsong@ictp.it

vibration by the amplitude x. While two position-dependent inverse capacitances $C_{\pm}^{-1}(x)$ of the parallel-plate capacitors are given by a linear function of x, the tunnel resistances of the air gap $R_{\pm}(x)$ exponentially depend on the width of the barrier: $C_{\pm}(x) = C_0 D/(D \mp x), R_{\pm}(x) = R_0 e^{\mp x/\lambda}$. Here, C_0 (R_0) is capacitance (resistance) of air gap of the width D, and λ is a phenomenological tunneling length. The force acting on the cantilever is the vector sum of electrostatic force applied to the end of the cantilever and Lorentz force induced by magnetic field $\vec{B} = B_0 \vec{e}_y$. The current I through the cantilever and the induced bias across the junction V_c satisfies the Ohm's law: $I = (V - V_c)/R_w$. We use following notations: R_w is resistance of the cantilever, $V_c = Q_c/C(x)$, Q_c is total charge accumulated inside the parallel-plate capacitors, and $C(x) = C_+(x) + C_-(x)$. Time evolution of the charge accumulated inside the parallel-plate capacitors can be written as

$$\dot{Q}_c + \left(\frac{1}{\tau_c(x)} + \frac{1}{\tau_w(x)}\right) Q_c - \frac{V}{R_w} = 0, \tag{1}$$

where $\tau_c(x) = R(x)C(x)$ is a position-dependent RC-time of the tunnel junction, $\tau_w = R_w C(x)$. Here, $R(x) = [1/R_+(x) + 1/R_-(x)]^{-1} = R_0(2\cosh(x/\lambda))^{-1}$. Then, the electrostatic force applied to the cantilever is given by $\vec{F}_c = -(Q_c)^2 (\partial C^{-1}(x)/\partial x)/2 \cdot \vec{e}_x$, and the effective Lorentz force induced by the current is $\vec{F}_b = L\vec{I} \times \vec{B}$. Thus, the equation of motion for the vibrating cantilever within the air gap along $\hat{x}$-direction is given by

$$\ddot{x} + 2\gamma_0 \dot{x} + \omega_0^2 x = a_1 \frac{Q_c^2}{C_0 D^2 m} x + a_2 \frac{LB_0}{mR_w}(V - V_c), \tag{2}$$

where m is the effective mass, ω_0 is a frequency of fundamental mechanical mode, and γ_0 is its damping coefficient. Here, a_1 and $a_2 \sim 1$ are geometrical factors.

In order to present a system of coupled equations describing both mechanical motion and charge distribution in compact form, we introduce dimensionless variables, denoted by tilde, which are defined by re-scaling the displacement with λ, the time with ω_0^{-1}, the current with $e\omega_0$, the voltage with e/C_0, and the force with $m\omega_0^2\lambda$ ($\tilde{x} = x/\lambda$, $\tilde{t} = \omega_0 t$, $\tilde{q}_c = Q_c/e$, $\tilde{I} = I/e\omega_0$, $\tilde{v} = C_0 V/e$, and $\tilde{F} = F/m\omega_0^2\lambda$)

$$\ddot{\tilde{x}} + \frac{1}{Q_0}\dot{\tilde{x}} + \tilde{x} = \frac{\alpha}{d^2}\tilde{q}_c^2 \tilde{x} + \frac{\pi\beta\phi_B}{\tau_0 r_w}(\tilde{v} - \tilde{q}_c), \tag{3}$$

$$\dot{\tilde{q}}_c + \frac{1}{\tau_0 r_w}(r_w \cosh(\tilde{x}) + 1)\tilde{q}_c = \frac{\tilde{v}}{\tau_0 r_w}, \tag{4}$$

with $\tau_0 = \omega_0 R_0 C_0$, $d = D/\lambda$, $r_w = R_w/R_0$, $1/Q_0 = 2\gamma_0/\omega_0$. Here, $\phi_B = \lambda L B_0/(h/e)$ is dimensionless flux through the area of triangle with linear sizes determined by the length of the cantilever and amplitude of mechanical vibration measured in the units of flux quantum $\phi_0 = h/e$. The dimensionless parameters α and β correspond to the charging energy $E_c = e^2/C_0$, and oscillator (zero point motion) energy $E_{\text{osc}} = \hbar\omega_0$ measured in units of elastic energy $E_e = m\omega_0^2\lambda^2$: $\alpha = a_1 E_c/(m\omega_0^2\lambda^2)$, $\beta = a_2 E_{\text{osc}}/(m\omega_0^2\lambda^2)$. Note that dimensionless RC-time τ_0 appears in Eq. (3) due to rescaling of voltage with the charging energy which is a "natural" unit for rescaling in Eq. (4). We ignore the bending effects of the cantilever inside the area between source and drain(s), and, assuming that the condition $\tilde{x}/d \ll 1$ is satisfied, disregard the corrections of the order of $(\tilde{x}/d)^2$ in Eqs. (3) and (4).

Two terms in the r.h.s. of Eq. (3) account for the retardation effects due to redistribution of charge and the Lorentz force acting on the moving cantilever. In the adiabatic limit $\tau_0 \ll 1$, we assume that the dynamics of the charge distribution is determined by RC-time, which is much faster compared to the time scales responsible for dynamics of mechanical degrees of freedom. The approximate analytic solution of Eq. (4) describes the position-dependent charge distribution, $\tilde{q}_c(\tilde{x})$

$$\tilde{q}_c(\tilde{x}) = \frac{\tilde{v}}{r_w \cosh(\tilde{x}) + 1}. \tag{5}$$

As one can see from Eq. (5), the charge accumulated at the tip of the cantilever decreases exponentially with the amplitude $\tilde{x}$.

First, let us consider the setup in the absence of perpendicular magnetic fields, $B = 0$ (see also Ref. 16). Then, the effective electromechanical potential can be written as $U_{\text{eff}}(\tilde{x}) = \frac{1}{2}\tilde{x}^2 - \frac{\alpha}{d^2}\tilde{v}^2 \int (r_w \cosh(\tilde{x}) + 1)^{-2} d\tilde{x}$. The values of two local minima $\tilde{x}_{\pm}$ are found by solving equation $\partial_x U_{\text{eff}}(\tilde{x}) = 0$. The solution reads $\tilde{x}_{\pm} = \pm\cosh^{-1}((\tilde{v}\sqrt{\alpha/d^2} - 1)/r_w)$. The emergence of $\tilde{x}_{\pm}$ gives us the condition for threshold bias ($\tilde{v}_1$) necessary for formation of a double-well shaped U_{eff}, which is written as $\tilde{v}_1 > (r_w + 1)/\sqrt{\alpha/d^2}$.

Nonadiabatic correction to the adiabatic charge

$$\tilde{q}_c^{na} = \frac{\tilde{v} r_w^2 \tau_0 \sinh(\tilde{x})}{(r_w \cosh(\tilde{x}) + 1)^3}\dot{\tilde{x}} \tag{6}$$

generates effective "negative" friction in the vicinity of the minima of the double-well potential. As a result, further increase of bias gives rise to instability of the static state. Finite energy pumping generates limit cycle at the vicinity of two local minima depending on the initial condition. With growing bias voltage, the two limit cycles evolve into one large limit cycle enveloping two local minima. This happens when the energy pumping allows the system to overcome the barrier between two local wells. Since there are two characteristic voltages controlling the number of limit cycles of the system, it is convenient to introduce two other critical voltages, $\tilde{v}_2$ and $\tilde{v}_3$, for two limit cycles and one limit cycle, respectively. General expressions for $\tilde{v}_2$ and $\tilde{v}_3$ are unavailable, however, we evaluate the characteristic voltages with assuming $r_w \ll 1$.[17]

The main focus of this paper is to demonstrate the re-switching behaviour of active device in the situation when the current injected mainly in the drain1 is eventually forced to be injected to the drain2. This is why we will be interested in the calculation of the difference between the current injected from the source to each of the drains, calling the current through the drain1 as I_+ and the drain2 as I_- (Fig. 1(a)). The difference between these two currents, which we call a "re-switching current" $\tilde{I}_{\text{diff}}$, can be fine-tuned by applying external magnetic field. The current $\tilde{I}_{\text{diff}}(\tilde{t}) = \tilde{I}_+(\tilde{t}) - \tilde{I}_-(\tilde{t})$ fully describes switching properties of the active device. It is convenient to characterize switching by

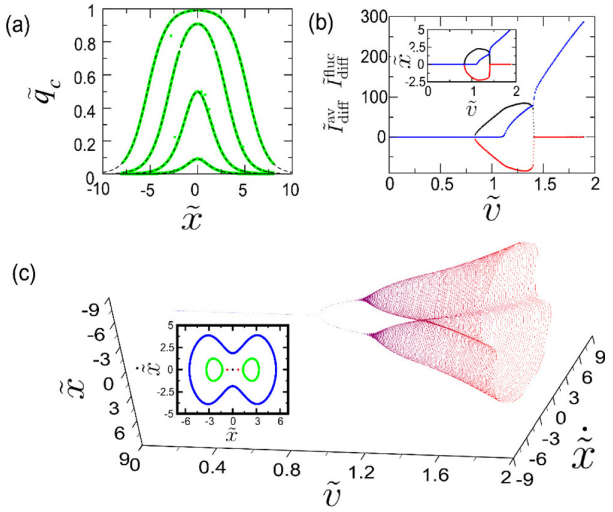

FIG. 2. (a) Charge distribution $\tilde{q}_c$ given by Eq. (5) (black dashed lines) and Eqs. (3) and (4) (green dots). The parameter $r_w = 1$, 0.1, 0.01, and, 0.001 (from top to bottom), we use $\tilde{v} = 1$ and $\alpha/d^2 = 1.75$. (b) The re-switching current $\tilde{I}^{av}_{diff}$ (black and red lines) defined as the current difference between source-drain1 and source-drain2 and its fluctuations $\tilde{I}^{fluc}_{diff}$ (blue line) averaged over the time interval $T = 1000\omega_0^{-1}$ (two different colors for re-switching current correspond to two different initial conditions: black—oscillation near drain1 $\tilde{x}_{int} = 0.1$ and red—oscillations near drain2, $\tilde{x}_{int} = -0.1$) as a function of bias. Inset: averaged displacement relative to symmetric position of the cantilever and its fluctuations. (c) Poincaré map of $(\tilde{x}, \dot{\tilde{x}})$ for the steady state at zero magnetic field $B = 0$ evaluated after delay time ($t > 5000\,\omega_0^{-1}$) as a function of bias voltage. Inset: cross section of main plot at the bias voltages $\tilde{v} = 0.8$ (black dot), 0.85 (two red dots), 1.2 (two green curves), and 1.6 (blue curve). The parameters are $\tau_0 = 0.1$, $\beta = 0.01$, and $Q_0 = 100$. In order to calculate (a) and (c), we choose 150 random initial conditions in the range of $(\tilde{x}_{int}, \dot{\tilde{x}}_{int}, \tilde{q}_{c\,int}) \in [-5, 5]$.

the current averaged over a time interval T being large compared to the period of mechanical vibrations (in the numerical calculations, we use $T = 1000\,\omega_0^{-1}$). Another important for switching dynamics time scale is associated with the delay t after which we perform the time averaging ($t > 5000\,\omega_0^{-1}$) in the steady state (see Fig. 2(b)). For $\tilde{v}_1 \le \tilde{v} \le \tilde{v}_3$, the difference $\tilde{I}^{av}_{diff}$ splits following the evolution of the system and depending on the initial condition either to the right ($\tilde{x}_{int} > 0$, black color in Fig. 2(b)) or to the left ($\tilde{x}_{int} < 0$, red color) near one of two minima of the potential $U_{eff}(\tilde{x})$. The shuttling regime ($\tilde{v}_2 \le \tilde{v}$) is characterized by non-zero fluctuations of the current difference, $\tilde{I}^{fluc}_{diff} = \langle \tilde{I}_{diff}(\tilde{t}) - \tilde{I}^{av}_{diff} \rangle$. The fluctuation strength continues to increase after a sudden drop of $\tilde{I}^{av}_{diff}$ at $\tilde{v}_3$ (see the blue line in Fig. 2(b)). The stationary Poincaré map of various random initial condition for $(\tilde{x}, \dot{\tilde{x}})$ as a function of $\tilde{v}$ is shown in Fig. 2(c). The one-to-one correspondence between the re-switching current and displacement shown in Fig. 2(b) can be used for position detection of the nano-device.

Next, we describe the setup in the presence of perpendicular magnetic field applied in order to manipulate the switching current between source and one of two drains, $\tilde{I}_{\pm}$ in the $\tilde{v}_1 \le \tilde{v} \le \tilde{v}_3$ regime. We consider adiabatically varying time-dependent flux $\phi_B(\tilde{t}) = \frac{b_0}{2}\left(\tanh\left(\frac{\tilde{t}-\tilde{t}_s}{\tau_p}\right) - \tanh\left(\frac{\tilde{t}-\tilde{t}_e}{\tau_p}\right)\right)$, under following condition for duration of the flux pulse $\tau_d = \tilde{t}_e - \tilde{t}_s$ and saturation time τ_p compared to the *RC*-time τ_0: $1/Q_0 < \tau_0 \ll \tau_d \ll \tau_p$. Figs. 3(a)–3(d) illustrate switching

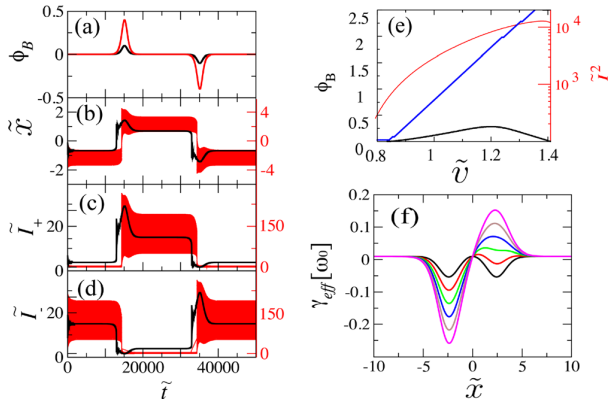

FIG. 3. Switching behavior of the device controlled by magnetic pulses. Time scanning of ϕ_B (a), $\tilde{x}$ (b), $\tilde{I}_+$ (c), and $\tilde{I}_-$ (d) at the bias voltage $\tilde{v} = 0.85$, $b_0 = 1$ (black), and $\tilde{v} = 1.2$, $b_0 = 4$ (red). (e) Critical magnetic field ϕ_B^{min} (black) and ϕ_B^{max} (blue) for switching phenomenon as a function of bias and the mean-square of the total current averaged at the critical value of magnetic field (red). (f) Position-dependent effective friction under different values of dimensionless flux ϕ_B from its minimal valued 0 (black) to maximum value 5 (magenta) with the step $\Delta\phi_B = 1$.

dynamics of a system initially located in the left minimum. We apply pulses $\tau_d = 200$ and $\tau_p = 1000$ at $\tilde{t}_s = 15000$ ($\tilde{t}_e = 35000$) for stimulating jumps from the left well to the right one and back. The voltage dependence of the lower/upper critical fields is shown in Fig. 3(e). If the magnetic field exceeds its upper critical limit, the double-well potential transforms into the single-well potential (Fig. 4(b)). The voltage dependence of the upper critical flux ϕ_B^{max} can be obtained by evaluating the minima of confining potential under condition that two stable minima transfer into single stable minimum. The lower critical field ϕ_B^{min} have been numerically defined as the minimal value of applied flux by comparing $\tilde{x}$ averaged over long time scale T before and after stimulation. In Fig. 3(e), red colored line shows log-scaled current square average, $\langle |\tilde{I}_+(\tilde{t}) + \tilde{I}_-(\tilde{t})|^2 \rangle$ at the ϕ_B^{min}, which is directly proportional to current power. It is therefore demonstrated that there exist regimes when small

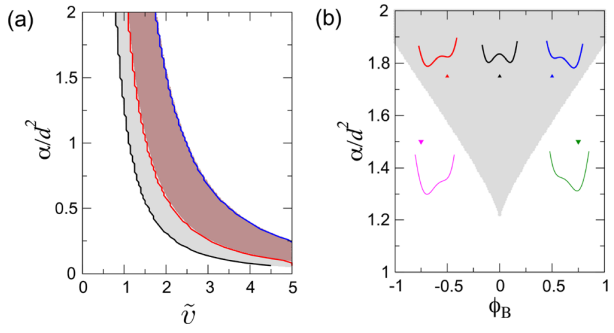

FIG. 4. Phase diagram for bi-stability in the parameter domain $(\tilde{v}, \alpha/d^2)$ under $\phi_B = 0$ for (a) and $(\phi_B, \alpha/d^2)$ with $\tilde{v} = 1$ for (b) by using adiabatic approximation (Eq. (5)). The brown colored area in (a) represents the shuttling-promoted switching regime, $\tilde{v}_2 < \tilde{v} < \tilde{v}_3$. Thick lines denote numerical solution of Eqs. (3) and (4) describing the evolution of critical voltages $\tilde{v}_1$ (black), $\tilde{v}_2$ (red), and $\tilde{v}_3$ (blue) as a function of applied bias $\tilde{v}$. The shape of electromechanical potentials in (b) corresponds to the points $\phi_B = 0$ (black), -0.5 (red), and 0.5 (blue) at $\alpha = 1.75$, and $\phi_B = -0.75$ (magenta), 0.75 (green) at $\alpha = 1.5$.

magnetic field can switch large currents in the active regime of nano-device due to amplification of device sensitivity by the preceding signal. As is seen from Fig. 3(e), small flux switches between two different regimes both at the voltages around $\tilde{v}_1$ and $\tilde{v}_3$. We emphasize the high sensitivity of Y-switch device to small variation of the magnetic field close to critical voltages $\tilde{v}_1$ and $\tilde{v}_3$.

The switching mechanism based on magnetic fields in the device can be considered by using position-dependent effective dissipation coefficient. Since the device shows position-dependent charge distribution, the Lorentz force involves non-adiabatic corrections to charge dynamics. Consequently, position-dependent effective dissipation has been emerged in the equation of motion

$$\gamma_{\text{eff}}(\tilde{x}) = \gamma_0 + \frac{\pi\beta\omega_0\tilde{v}\phi_B r_w \sinh(\tilde{x})}{(r_w\cosh(\tilde{x})+1)^3} - \frac{2\alpha\omega_0\tau_0}{d^2}\frac{\tilde{v}^2 r_w^2 \tilde{x}\sinh(\tilde{x})}{(r_w\cosh(\tilde{x})+1)^4}.$$

Fig. 3(f) shows position-dependent $\gamma_{\text{eff}}(\tilde{x})$ as a function of varying magnetic field. Unlike the Lorentz force, which is an odd function of the coordinate $\tilde{x}$, flux ϕ_B, and voltage $\tilde{v}$, the non-adiabatic contribution to the electrostatic force being even function of both coordinate $\tilde{x}$ and bias voltage $\tilde{v}$ always reduces the dissipation near stationary position.

Using adiabatic approximation, we calculate the phase diagrams of bi-stability regime (see Fig. 4), from which the potentialities of current switch can be seen. We use the following color scheme in Fig. 4(a): gray color is used for "*passive*" switching regime $(\tilde{v}_1 < \tilde{v} < \tilde{v}_2)$ and brown color denotes the "*active*" switching regime based on the shuttling instability $(\tilde{v}_2 < \tilde{v} < \tilde{v}_3)$.

In conclusion, we have reported current-switching device promoted by shuttling phenomenon based on magnetically controllable bi-stability based on strong NEM coupling. In contrast to Ref. 14 implementing the static 3-terminal Y-switch, our 3-terminal system containing movable source possesses one more fine-tuning parameter, namely, magnetic field controlling the switching regime. The NEM coupling gives rise to double-well shaped electromechanical potential controlled by bias voltage. We have performed both numerical and analytical analysis and found regime of shuttling instability. In the above analysis, we ignore the fluctuations of displacement and voltage, which can be generated by both mechanical and electrical noise. The fluctuations of the cantilever displacement should be essentially smaller than the inter-valley distance, which should be of the order of tunneling length to have a high on/off ratio. Our analysis shows that as this condition is fulfilled, the voltage fluctuation are negligible compared to $\tilde{v} - \tilde{v}_c \sim \tilde{v}_c$. At the typical experimental parameters, the corresponding restriction reads $T \ll 100\,\text{K}$. At high temperatures, the fluctuation become important and can generate a number of phenomena similar to noise-enhanced stability[18,19] and stochastic resonance.[20,21]

We appreciate fruitful discussions with K.-H. Ahn, Hee Chul Park, and S. Ludwig. The research of K.K. was partially supported by ISF Grant No. 400/12. The work of R.I.S. and L.Y.G. was supported in part by Swedish VR.

[1]M. Blencowe, Phys. Rep. **395**, 159 (2004).
[2]M. Poot and H. S. J. van der Zant, Phys. Rep. **511**, 273 (2012).
[3]R. I. Shekhter, Zh. Eksp. Teor. Fiz. **63**, 1410 (1972).
[4]T. K. Ng and P. A. Lee, Phys. Rev. Lett. **61**, 1768 (1988).
[5]G. Weick, F. von Oppen, and F. Pistolesi, Phys. Rev. B **83**, 035420 (2011).
[6]D. Fedorets, L. Y. Gorelik, R. I. Shekhter, and M. Jonson, Phys. Rev. Lett. **95**, 057203 (2005).
[7]F. Pistolesi, Y. M. Blanter, and I. Martin, Phys. Rev. B **78**, 085127 (2008).
[8]L. Y. Gorelik, A. Isacsson, M. V. Voinova, B. Kasemo, R. I. Shekhter, and M. Jonson, Phys. Rev. Lett. **80**, 4526 (1998).
[9]R. I. Shekhter, L. Y. Gorelik, I. V. Krive, M. N. Kiselev, A. V. Parafilo, and M. Jonson, Nanoelectromech. Syst. **1**, 1 (2013).
[10]H. Park, J. Park, A. K. L. Lim, E. H. Anderson, A. P. Alivisatos, and P. L. McEuen, Nature **407**, 57 (2000).
[11]A. Erbe, C. Weiss, W. Zwerger, and R. H. Blick, Phys. Rev. Lett. **87**, 096106 (2001).
[12]D. V. Scheible and R. H. Blick, Appl. Phys. Lett. **84**, 4632 (2004).
[13]C. Kim, M. Prada, and R. H. Blick, ACS Nano **6**, 651 (2012).
[14]C. Kim, H.-S. Kim, M. Prada, and R. H. Blick, Nanoscale Commun. **6**, 8571 (2014).
[15]F. Santandrea, L. Y. Gorelik, R. I. Shekhter, and M. Jonson, Phys. Rev. B **85**, 205408 (2012).
[16]A. Isacsson, Phys. Rev. B **64**, 035326 (2001).
[17]See supplementary material at http://dx.doi.org/10.1063/1.4931458 for computing details of two critical voltage V_2 and V_3.
[18]N. V. Agudov and B. Spagnolo, Phys. Rev. E **64**, 035102 (2001).
[19]A. Fiasconaro, B. Spagnolo, and S. Boccaletti, Phys. Rev. E **72**, 061110 (2005).
[20]L. Gammaitoni, P. Hänggi, P. Jung, and F. Marchesoni, Rev. Mod. Phys. **70**, 223 (1998).
[21]R. N. Mantegna and B. Spagnolo, Phys. Rev. E **49**, R1792 (1994).